Improved dq model and analytical parameters determination of a Permanent Magnet Assisted Synchronous Reluctance Motor (PMa-SynRM) under saturation using Frozen Permeability Method

Jessica Neumann, Carole Hénaux, Maurice Fadel, Dany Prieto, Etienne Fournier, Mathias Tientcheu Yamdeu

Improved dq model and analytical parameters determination of a Permanent Magnet Assisted Synchronous Reluctance Motor (PMa-SynRM) under saturation using Frozen Permeability Method

J. Neumann, C. Hénaux, M. Fadel, D. Prieto, E. Fournier, M. Tientcheu Yamdeu

***Abstract*–The classic dq model does not take into account the machine's saturation and cross magnetization. This paper presents an improved dq model and a new technique to determine the electromagnetic parameters of a PMa-SynRM under saturation condition. These parameters are computed by means of an upgraded analytical magnetic model of the motor and the Frozen Permeability Method (FPM) is applied to separate the magnetic field sources effects, keeping the same magnetic state of the steel sheets as the one at the operation point. Permanent magnet flux in both dq-axis, apparent and incremental inductances are determined and they are implemented in a complete dq model. This model is validated by means of an accurate representation of PWM harmonics in relation to a numerical model implemented in Matlab/Simulink where the motor is represented by a flux map.**

***Index Terms* — dq model, frozen permeability method, magnetic analytical model, PMa-SynRM, incremental inductances, apparent inductances, permanent magnet flux, crossing magnetization, saturation**

I. NOMENCLATURE

I_d, I_q: dq current components
λ_d, λ_q: dq linkage flux components
v_d, v_q: dq voltage components
L_d, L_q: dq self-apparent inductances components
L'_d, L'_q: dq incremental inductances components
M_{dq}, M_{qd}: dq crossing magnetization apparent inductances components
M'_{dq}, M'_{qd} : dq incremental crossing magnetization inductances components
p: number of pairs of poles
f: electrical frequency
ω: electrical pulsation
K: winding constant
N_t: winding turns number per pole and phase
I_s: current crossing a stator slot
N_c: number of conductors per slot
α: current angle
θ: rotor position
τ: slot pitch
w: stator tooth width
R_{yoke}: yoke medium radius
h_{yoke}: stator yoke height

II. INTRODUCTION

PERMANENT magnet synchronous motors are widely used due to their high performance and high torque density. An alternative that has proven even more interesting is the Permanent Magnet Assisted Synchronous Reluctance Motor (PMa-SynRM), since its reluctance torque allows the usage of cheaper magnets, keeping the same performance and power factor [1].

Fast and precise computation of dq parameters of PMa-SynRMs is necessary to estimate its performance as well as to run its control algorithms [2]. To compute these parameters, the non-linearity of the steel sheets has to be taken into account in the magnetic model of the machine. Parameters also change with the operating point. For example, permanent magnet flux at no-load condition is not the same as at load operation. The saturation at load operation impact in the same way the inductances. Therefore, the classical way of parameters computation and the classic dq model have to be upgraded.

In section III of this paper, the analytical magnetic model of the motor and its improvements are presented. This model was developed in previous work [3] and it is based on Maxwell equations, more specifically Ampère's theorem and magnetic flux conservation law. Fig. 1. presents the modeled motor, which has a structure of four poles and three flux barriers per pole filled with Neodymium Iron Boron (NdFeB) magnets.

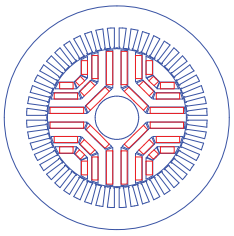

Fig. 1. Transversal section of the PMa-SynRM

Section IV presents an approach to compute the parameters of the machine at load operation. To separate the magnetic field sources (magnets and current) in a non-linear system like PMa-SynRMs, the Frozen Permeability Method (FPM) is used. Differently of several authors [4]-[8], that use FPM implemented in Finite Elements (FE) software, in this work the FPM is implemented in the analytical magnetic model of the motor described in section III and is used to determine self and crossing magnetization dq inductances as well as the magnetic flux of the

J. Neumann is with Laplace, University of Toulouse and Leroy Somer – Nidec, Toulouse, 31071 France (email: neumann@laplace.univ-tlse.fr)
C. Hénaux is with Laplace, University of Toulouse, Toulouse, 31071 France (henaux@laplace.univ-tlse.fr)
M. Fadel is with Laplace, University of Toulouse, Toulouse, 31071 France (fadel@laplace.univ-tlse.fr)
D. Prieto is with Leroy Somer - Nidec, Angoulême, 16000 France (e-mail: dany.prieto@mail.nidec.com)
E. Fournier is with Leroy Somer - Nidec, Angoulême, 16000 France (e-mail: etienne.fournier@mail.nidec.com)
M. Tientcheu Yamdeu is with Leroy Somer - Nidec, Angoulême, 16000 France (e-mail: mathias.tientcheuyamdeu@mail.nidec.com)

magnets in both dq-axis.

In section V, an adapted dq model based on [9] and [10] is detailed. Contrary to the classic model, not only the self-apparent inductances and the magnet's flux oriented according to the d-axis are considered. In this model the terms of cross magnetization, previously calculated by FPM, are included and the definition of incremental inductance is associated with the dynamic term di/dt in the $v_{d,q}$ equations. Reference [11] shows that in a state of saturation the values of incremental and apparent inductances are no longer equal. The accuracy of the proposed model is proven by a comparison with a numerical model implemented in Matlab/Simulink.

III. ANALYTICAL MODEL

The analytical magnetic model of the machine is based on a system of equations written from the Ampère's closed circuits as shown in Fig. 2., together with the flux conservation laws applied between the flux barriers and the constitutive expressions of the materials [3]. The system is solved for each θ_i in order to obtain the airgap flux density along a pair of poles. Once it has been determined, it is possible to calculate the parameters and performances of the motor.

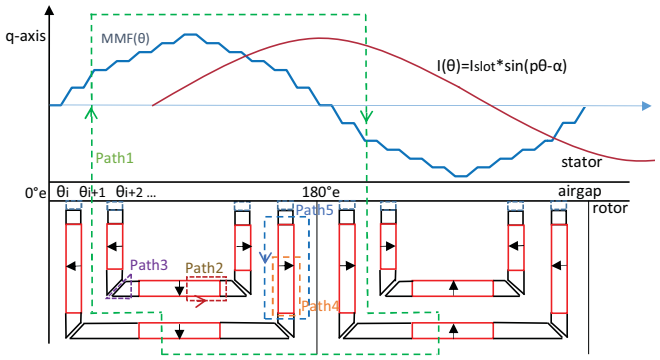

Fig. 2. Ampère's circuits in one pair of poles of the motor

A. Magnetomotive Force (MMF)

Initially [2] represents the MMF of the stator (involved by the green circuit in Fig. 2.) by its harmonic expression, and only the fundamental component is considered, with its amplitude is described as (1)

$$mmf_1 = \frac{3\sqrt{2}}{\pi p} K N_t I \tag{1}$$

For a better accuracy, the model is completed by constructing the true MMF waveform, where space harmonics from the current distribution can therefore be taken into account. The studied machine has a distributed and diametric pitch winding and it can be represented as in Fig. 3.a.

By browsing θ for a given point in time (for example t=0s), the three phase currents in (2) are computed and the MMF is obtained from the sum of the contribution of the Ampère-turns ($N_c \times I_s$) of each slot showed in Fig. 3.b

$$\begin{aligned} I_a &= \mathrm{I}\cos(\omega t) \\ I_b &= \mathrm{I}\cos(\omega t + \frac{2\pi}{3}) \\ I_c &= \mathrm{I}\cos(\omega t + \frac{4\pi}{3}) \end{aligned} \tag{2}$$

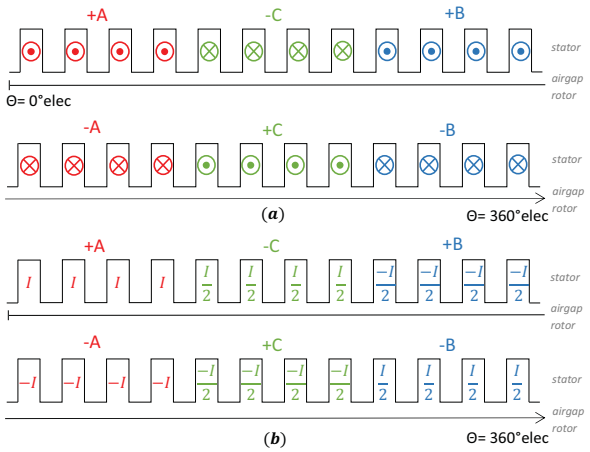

Fig. 3. Schematic of stator winding (a) slot position of each phase (b) slot currents at t=0s

A better representation of the MMF provides more accuracy to compute the airgap flux density waveform. Knowing the values of harmonics of the airgap flux density allows the estimation of the iron losses in the material of the machine.

Fig. 4 compares the airgap flux densities obtained by the FE model (blue curve), the analytical model with the fundamental of the MMF (black curve) and the analytical model taking account the true MMF waveform (red curve). In order to observe only the influence of the MMF, the machine is simulated with a solid rotor, i.e. there are no magnets or reluctance in the rotor. The material of the sheets is also considered linear and the slot openings in the stator are reduced.

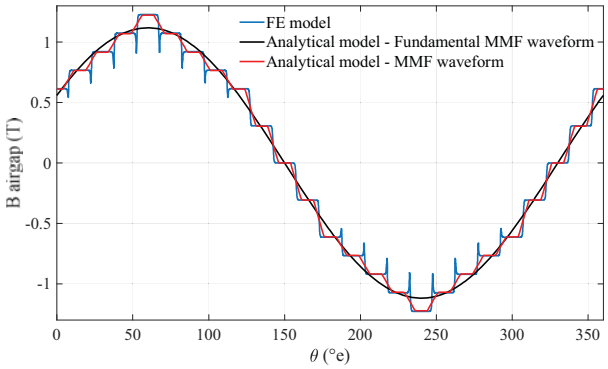

Fig. 4. Comparison of airgap flux density waveform for different ways of MMF representation

As shows Table I, the winding harmonics of rang 1, 3, 5, 9, 11 and 13 are very well represented when the MMF waveform is included, with maximum error of 9%.

TABLE I
MMF HARMONICS PRESENT IN THE AIRGAP FLUX DENSITY

Harmonic	FE model	Analytical model with fundamental of MMF (T)	Error (%)	Analytical model with MMF waveform(T)	Error (%)
1	1.110	1.119	0.8	1.118	0.7
5	0.048	-	-	0.047	2
7	0.026	-	-	0.025	4
11	0.013	-	-	0.012	8
13	0.011	-	-	0.010	9
17	0.011	-	-	0.009	18
19	0.013	-	-	0.010	23
23	0.061	-	-	0.034	44
25	0.031	-	-	0.030	3

The harmonics in the airgap flux density are also present in the flux density in the material of the stator teeth and yoke due to the flux conservative law which allows to establish (3) and (4).

$$B_{tooth}(\theta) = \frac{\tau}{w} B_{airgap}(\theta) \tag{3}$$

$$B_{stator\ yoke}(\theta) = \frac{R_{yoke}}{2h_{yoke}} \int_{\theta}^{\theta+180^\circ} B_{airgap}(\theta)\, d\theta \tag{4}$$

The amplitude of the space harmonics in Table I may not seem important, however they contribute significantly in the iron losses of the machine, as they are proportional to the square of the electrical frequency.

B. *Inclination of flux barriers*

As shown in [12] for two different structures of PMa-SynRMs, adding an inclination angle (δ) to the flux barriers improves the sensorless capability of the machine and can also improve the torque. Four and six-poles motors were analyzed, for the first one the sensorless capability was improved in 5% and for the second structure the sensorless and torque were improved in 28% and 5% respectively.

This angle (δ) is illustrated in Fig.5. and was added to the machine's geometry of the analytical model.

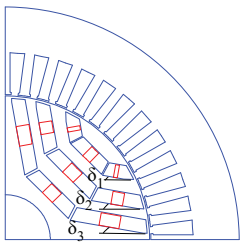

Fig. 5. Inclination angle of flux barriers

C. *Validation of the PMa-SynRM analytical model*

For means of comparison the PMa-SynRM is also modeled in the FEMM FE software [12].

Fig. 6. and Fig.7 compare the airgap flux density at no-load and load condition, respectively. The biggest difference between the two models is the drops of B_{airgap} in face of a stator slot. In the analytical model the airgap is pondered by the Carter's coefficient as an average airgap, and for this reason it does not take into account the slot openings. In both figures the fundamental of the flux density is plotted in dashed, and they match reasonably well with the FEMM results.

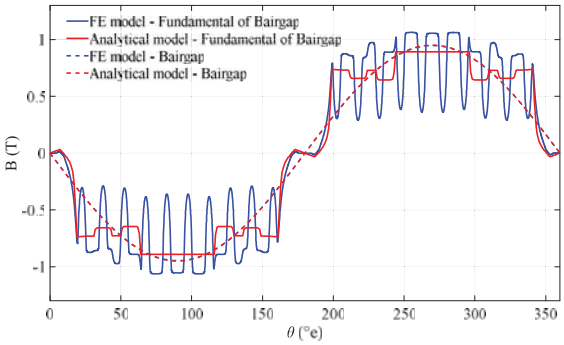

Fig. 6. Airgap flux density in no-load condition

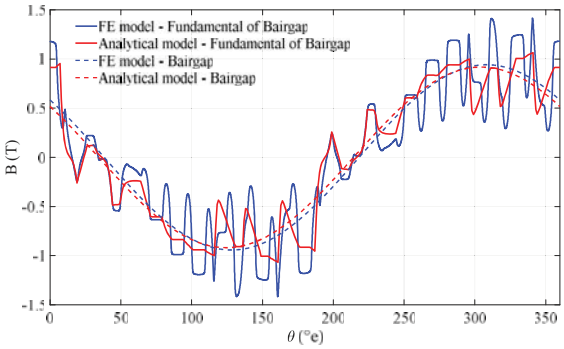

Fig. 7. Airgap flux density at 15A and current angle of 60°.

The torque and voltage at 15A obtained by the two models are plotted in relation to the current angle in Fig. 8.a. and Fig. 8.b. The maximum error for the torque and voltage are 6% and 5%, respectively.

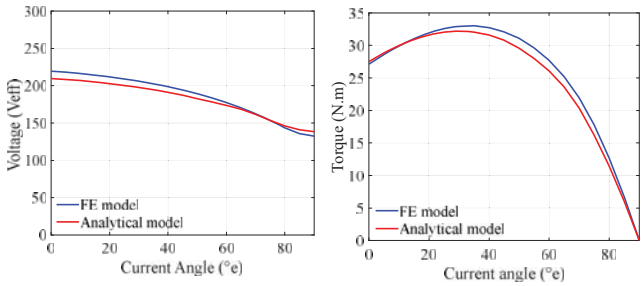

(a) (b)

Fig. 8. Comparison of FE and analytical model at 15A: (a) voltage x current angle and (b) torque x current angle.

IV. FROZEN PERMEABILITY

Due to the non-linearity of the steel sheet material it is not possible to segregate the field sources and analyze their effects independently. The FPM is therefore an alternative to linearize the system.

For one on load operating point (OP) of the machine, the flux density B_{OP} and magnetic field H_{OP} computed by the analytical model in each point of motor are placed in the BH curve of the steel sheet material, and the corresponding permeability (μ_{OP} in Fig.9.) is frozen. The next computations ($B_{PM(FPM)}$ and $B_{i(FPM)}$), where each field source (magnet and current) is considered separately, are done maintaining the same permeability μ_{OP}.

The OP chosen to illustrate the following analysis is the

nominal operating point of the motor – 15 A and current angle 60°. The airgap flux density calculated by the analytical model is represented by "OP" in Fig. 13., and the flux values are summarized in Table II.

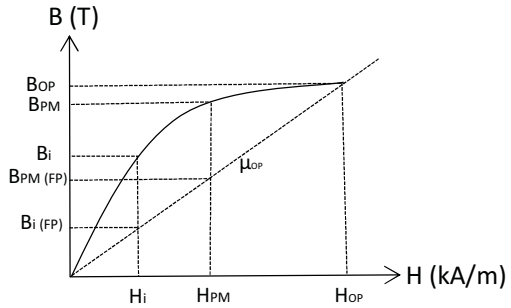

Fig. 9. Frozen permeability in the B(H) curve of the material

By separating the field sources and simulating the motor only with the permanent magnets (no current), and keeping the permeability μ_{OP}, it is possible to determine the real contribution of the magnets in the OP.

Table II compares the flux contribution of the permanent magnets calculated by the analytical model using FPM with a conventional computation at no-load condition. On the d-axis, there is a difference in the magnetic flux – the conventional computation gives 0.47 Wb and the FPM results in 0.51 Wb. With the FPM it is possible to see that the q-axis component is not negligible (0.13Wb) and it generates an important voltage component in d-axis (40.75 V). To visualize this phenomena, Fig. 10. illustrates the flux lines distribution of a no-load FE simulation and a FE simulation with FPM. In Fig.10.b, the saturation of the OP makes the flux lines generated by magnets not only create flux in the same axis, but it also produces flux in q-axis.

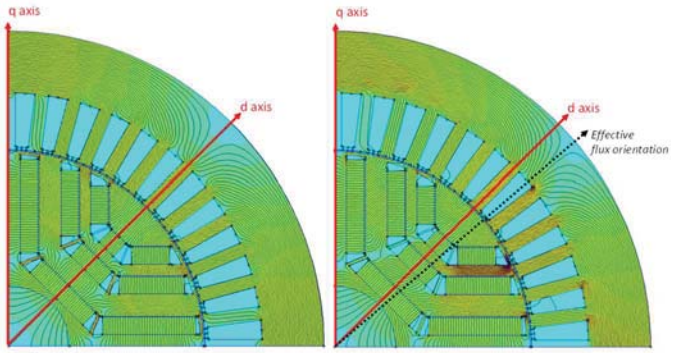

(a) (b)

Fig. 10. Flux density distribution: (a) no load condition and (b) simulation with only magnets being field source using FPM

The airgap flux density obtained with the analytical model for this case is plotted in Fig.13. and called "PM(FPM)".

TABLE II
DQ FLUX AND VOLTAGE COMPONENTS FOR CONVENTIONAL COMPUTATION AND FOR COMPUTATION USING FROZEN PERMEABILITY METHOD

	$\lambda_d(Wb)$	$\lambda_q(Wb)$	$v_d(V)$	$v_q(V)$
Combined - OP	0.37	0.26	-81.83	115.71
PM	0.47	0	0	148.51
Id	-0.15	0	0	-46.47
Iq	0	0.45	-140.25	0
PM (FPM)	0.51	-0.13	40.75	159.83
Id (FPM)	-0.16	-0.03	9.75	-50.30
Iq (FPM)	0.02	0.42	-130.16	5.69

The same procedure is done for the dq currents components. Each component is injected at a time, and the magnets are replaced by air. Similar to what happened previously, by keeping the magnetic state of the OP makes that injecting the current component I_d or I_q generates not only the magnetic flux oriented in the same axis but also in the other one. Fig. 11. and Fig. 12. illustrate the flux lines distribution obtained by FE simulation for I_d and I_q excitations respectively. Magnetic flux and voltage values computed with conventional method and FPM, are summarize in table II.

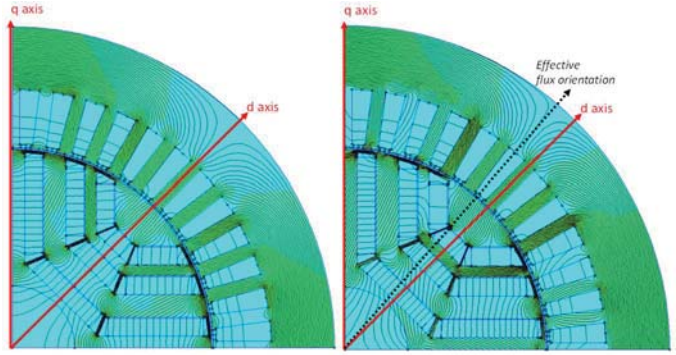

(a) (b)

Fig. 11. Flux density distribution: (a) d-current excitation and (b) d-current excitation using FPM

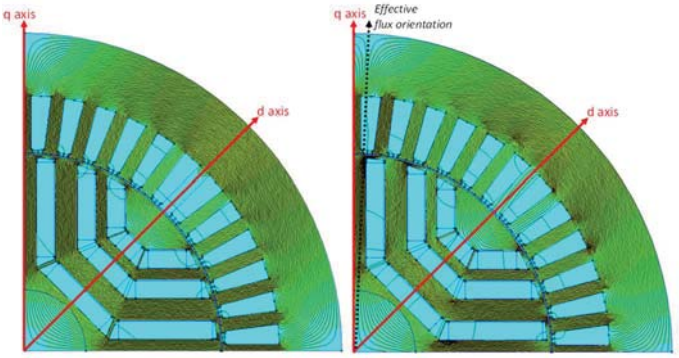

(a) (b)

Fig. 12. Flux density distribution: (a) q-current excitation and (b) q-current excitation using FPM

The airgap flux density contribution of each dq current component is plotted in Fig. 13. In the same figure, we can see that the FPM applied to the analytical model of the machine linearized the system, since the sum (dashed curve) of the airgap flux densities computed separately for each excitation is equal to the flux density calculated at the OP.

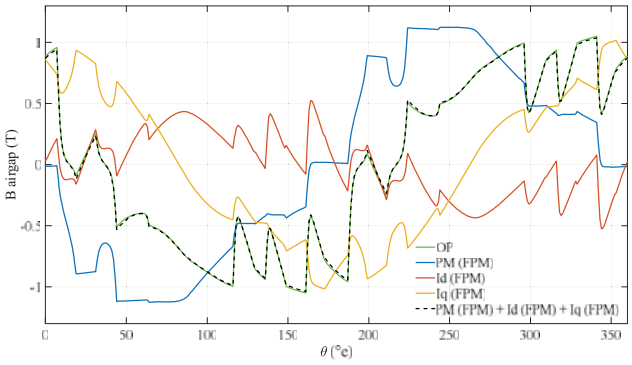

Fig. 13. Airgap flux density waveforms obtained by analytical model using FPM

V. PMA-SYNRM PARAMETERS COMPUTATION AND UPDATED DQ MODEL

A. Parameters computation and dq model

The classic dq model defines the voltage in the terminals of the machine in the Park referential as described in (5).

$$v_d = Ri_d + L_d\frac{di_d}{dt} - \omega_s L_q i_q$$
$$v_q = Ri_q + L_q\frac{di_q}{dt} + \omega_s(\lambda_d^{pm} + L_d i_d) \quad (5)$$

In this model, the magnetic flux of the permanent magnets is represented only by one component in the d-axis (term λ_d^{pm}), and it is computed by one simulation at no-load condition. Concerning the inductances, only the self-apparent inductances are taken into account and they are calculated as in (6). The magnetic flux produced by I_d is considered to be the difference between the total d-axis flux and the no–load magnet flux ($\lambda_d - \lambda_d^{pm}$).

$$L_d = \frac{\lambda_d - \lambda_d^{pm}}{I_d}$$
$$L_q = \frac{\lambda_q}{I_q} \quad (6)$$

As the saturation level becomes higher, all these assumptions are no more valid. Inductances are no longer constants and have to be computed at each working point. The effect of cross-coupling analyzed in section IV has also to be taken account.

Reference [10] does a preliminary study in a complete model as presented in (7)

$$v_d = Ri_d + L'_d\frac{di_d}{dt} + M'_{dq}\frac{di_q}{dt} - \omega_s(L_q i_q + M_{qd} i_d + \lambda_q^{pm})$$
$$v_q = Ri_q + L'_q\frac{di_q}{dt} + M'_{qd}\frac{di_d}{dt} + \omega_s(\lambda_d^{pm} + L_d i_d + M_{dq} i_q) \quad (7)$$

The equations for the inductances computation are listed in (8), where L_d and L_q are the self-apparent inductances and M_{dq} and M_{qd} are the crossing magnetization apparent inductances defined as the ratio of the flux generated in the d-axis by the current injected in the q-axis and vice versa, respectively.

The FPM implemented in the analytical magnetic model of the motor, as explained in section IV, allows the computation of the self and cross-magnetization inductances.

$$L_d = \frac{\lambda_d}{I_d} \qquad M_{dq} = \frac{\lambda_{dq}}{I_d}$$
$$M_{qd} = \frac{\lambda_{qd}}{I_q} \qquad L_q = \frac{\lambda_q}{I_q} \quad (8)$$

Differently from the classic model, (7) distinguish apparent inductances from incremental ones. Both can be considered equal only at no-saturate state. Reference [11] demonstrated how incremental inductance becomes different from apparent ones in saturation zone. The definition of incremental inductance is detailed in (9).

$$L'_d = \left.\frac{\Delta\lambda_d}{\Delta I_d}\right|_{I_q=cst} \qquad L'_q = \left.\frac{\Delta\lambda_q}{\Delta I_q}\right|_{I_d=cst}$$
$$M'_{dq} = \left.\frac{\Delta\lambda_d}{\Delta I_q}\right|_{I_d=cst} \qquad M'_{qd} = \left.\frac{\Delta\lambda_q}{\Delta I_d}\right|_{I_q=cst} \quad (9)$$

To determine the PMa-SynRM's parameters at the rating point of the machine, the values of the table II can be applied to the expressions in (8) and (9). For the incremental inductances the FPM is not used and ΔI_d and ΔI_d are equal to 2.12A (10% of the current pic value). The inductance values obtained from the upgraded and classic model are listed in Table III. The incremental crossing magnetization inductances are negative, it means that a positive variation of current on one of the dq axis reduces the magnetic flux in the other axis.

TABLE III
DQ MODEL PARAMETERS COMPUTED USING FPM AND INCREMENTAL INDUCTANCES

dq Model	L_d (mH)	L_q (mH)	M_{dq} (mH)	M_{qd} (mH)	L'_d (mH)	L'_q (mH)	M'_{dq} (mH)	M'_{qd} (mH)	λ_d^{pm} (Wb)	λ_q^{pm} (Wb)
Improved	8.7	39.1	1.7	1.7	11.9	4.7	-1.6	-1.2	0.51	-0.13
Classic	5.7	24.6	-	-	-	-	-	-	0.47	-

B. Improved dq model implementation

In order to validate the improved dq model, the current harmonics due to the PWM supply of the motor will be analyzed. This allows the evaluation of the model assumptions and the inductance values previously calculated.

Analytical expressions of v_d and v_q for a SVPWM (Space Vector Pulse Width Modulation) supply developed in [14] are replaced in (7) for the improved model and in (5) for the classic model. The system of equations for both models is solved in order to obtain the currents. The method called "dq Harmonic Balance" [15] is used to solve the system of equations, i.e. each voltage harmonic generates the same rank of current harmonic. For each operation point, the new parameters of the machine are calculated from the analytical magnetic model.

C. Comparison model

As a comparison model, the same system (inverter and motor) is implemented in Simulink/Matlab as shown in Fig.14. Simulink blocs generate the SVPWM commands for the inverter that delivers the requested three-phase voltage. This voltage is then transformed into the dq referential and from the relations in (10), v_d and v_q are transformed into λ_q and λ_d, which are input signals for the motor model.

$$\lambda_d = \int v_d - Ri_d + \omega\lambda_q \, dt$$
$$\lambda_q = \int v_q - Ri_q - \omega\lambda_q \, dt \quad (10)$$

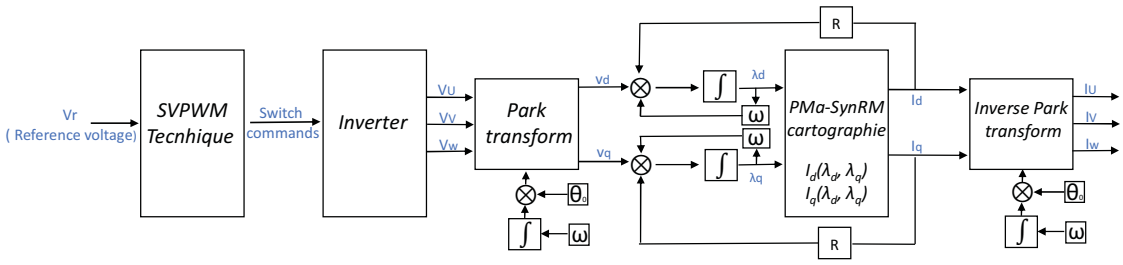

Fig. 14. Comparison model of the inverter plus motor in Simulink

In this schematic, the machine is represented by a cartography [16], i.e. a *current x magnetic flux* map that was previously built from FE simulations. Firstly, simulations for different combinations of (I_d,I_q) are carried out to build maps of λ_d and λ_q, both as a function of I_d and I_q. Thereafter these maps are numerically inverted to have I_d and I_q, both as a function of λ_d and λ_q. As these cartographies were obtained by FE simulation, the model is accurate and considers the saturation phenomena.

So, inside of Simulink software, the motor's model restores from the flux inputs signals (λ_q and λ_d) the corresponding currents components (I_d,I_q) by means of the Simulink lookup table function. The dq currents are then transformed to the three-phase referential and the harmonics can be analyzed.

Fig. 15 compares the current curves obtained for the three methods. The zoom of the selected part shows that the curve of the improved model is closer from the curve of Simulink/Matlab model than that obtained by the classic model.

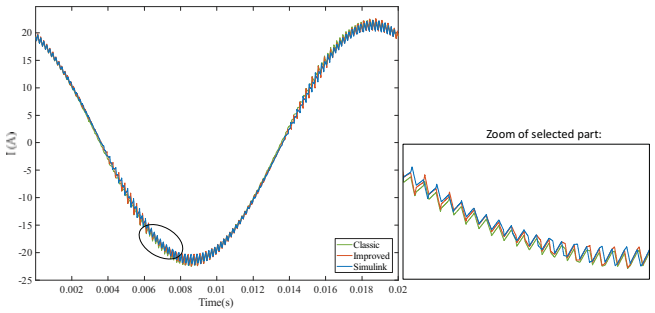

Fig. 15. Comparison of current waveforms obtains with classical improved and Simulink/Matlab model

For a better analysis of the harmonics representation, a Fourier transformation is applied to these curves. Fig.16.a. resumes the main harmonics amplitude, of which the fundamental value is 15 A. As the sampling frequency of the inverter is equal to 3kHz, the harmonics are around the multiple frequencies of it. For these simulations, the machine parameters of Table III are used.

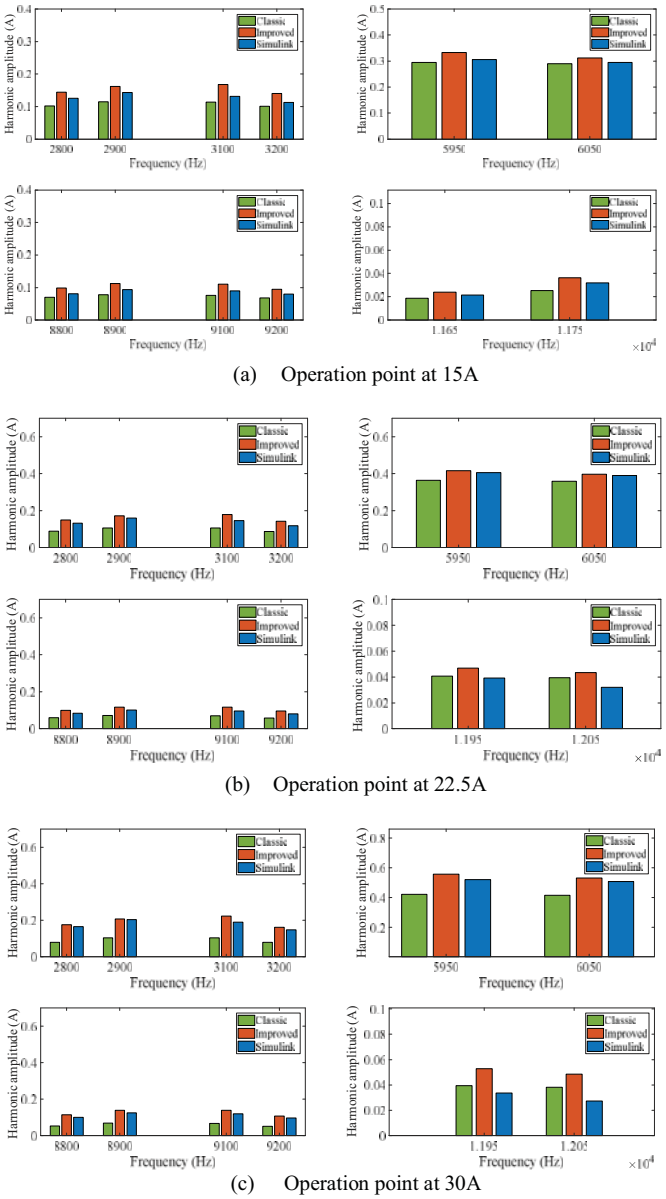

(a) Operation point at 15A

(b) Operation point at 22.5A

(c) Operation point at 30A

Fig. 16. PWM current harmonic amplitudes

At 15 A, the two models, classic and improved, are balanced and represent well the harmonics with an average absolute error of 13% and 17%. But as the current level increases, the improved model is much more accurate than the classic one as shown in Fig.16.b. and Fig16.c.,for operations at 22.5 A and 30 A, respectively. The absolute average error values for three different current levels are listed in Table IV. For 22.5 and 30 A, the new model keeps its error constant around 17%, while the classic model has errors of 24 and 40%.

TABLE IV
AVERAGE ERROR OF HARMONICS AMPLITUDE OF THE TWO MODELS FOR THE THREE OPERATION POINTS

Current level of the simulation (A)	15	22.5	30
Classic model (%)	12.56	23.74	40.28
Improved model (%)	17.21	16.04	17.06

VI. CONCLUSION

This paper presented an improved dq model and a new way of calculating the parameters applied for a PMa-SynRM.

The dq parameters of the machine are calculated from a precise analytical magnetic model. Recent improvements applied for this model were also presented and contrary to previous publications, this paper presents the FPM applied to an analytical model of the motor and crossing magnetization phenomena was evaluated and incorporated into the dq model.

The new dq model separates apparent and incremental inductances, considers the coupling terms and is updated at each point of operation with new inductances values and magnet flux. Compared to a model implemented in Simulink/Matlab were the machine's representation is based on FE simulations, it presented high precision and robustness for different current levels.

VII. REFERENCES

[1] S. S. Reddy Bonthu, M. Z. Islam, and S. Choi, "Performance Review of Permanent Magnet assisted Synchronous Reluctance Traction Motor Designs," in 2018 IEEE Energy Conversion Congress and Exposition (ECCE), 2018.

[2] N. Bianchi and S. Bolognani, "Magnetic models of saturated interior permanent magnet motors based on finite element analysis," in Conference Record of 1998 IEEE Industry Applications Conference. Thirty-Third IAS Annual Meeting (Cat. No.98CH36242).

[3] D. Prieto, P. Dessante, J.-C. Vannier, X. Jannot, and J. Saint-Michel, "Analytical model for a saturated Permanent Magnet Assisted Synchronous Reluctance Motor," in 2014 International Conference on Electrical Machines (ICEM), 2014.

[4] X. Chen, V. I. Patel, J. Wang, P. Lazari, L. Chen, and P. Lombard, "Reluctance Torque Evaluation for Interior Permanent Magnet Machines Using Frozen Permeability," in 7th IET International Conference on Power Electronics, Machines and Drives (PEMD 2014), 2014.

[5] X. Liu, H. Chen, J. Zhao, and A. Belahcen, "Research on the Performances and Parameters of Interior PMSM Used for Electric Vehicles," IEEE Transactions on Industrial Electronics, vol. 63, no. 6, pp. 3533–3545, Jun. 2016.

[6] E. SOKOLOV and M. MIHOV, "Parameter Estimation of an Interior Permanent Magnet Synchronous Motor," in 2019 16th Conference on Electrical Machines, Drives and Power Systems (ELMA), 2019.

[7] G. T. de Paula, J. R. B. de A. Monteiro, T. E. P. de Almeida, M. P. de Santana, and W. C. A. Pereira, "Evaluation of surface mounted PM machine's parameters on load conditions using Frozen Permeability Method. Part. I," in 2014 IEEE 23rd International Symposium on Industrial Electronics (ISIE), 2014.

[8] J. A. Walker, D. G. Dorrell, and C. Cossar, "Flux-linkage calculation in permanent-magnet motors using the frozen permeabilities method," IEEE Transactions on Magnetics, vol. 41, no. 10, pp. 3946–3948, Oct. 2005.

[9] S. Zarate, G. Almandoz, G. Ugalde, J. Poza, and A. J. Escalada, "Extended DQ model of a Permanent Magnet Synchronous Machine by including magnetic saturation and torque ripple effects," in 2017 IEEE International Workshop of Electronics, Control, Measurement, Signals and their Application to Mechatronics (ECMSM), 2017, doi: 10.1109/ecmsm.2017.7945881.

[10] A. Pouramin, R. Dutta, M. F. Rahman, J. E. Fletcher, and D. Xiao, "A preliminary study of the effect of saturation and cross-magnetization on the inductances of a fractional-slot concentrated-wound interior PM synchronous machine," in 2015 IEEE 11th International Conference on Power Electronics and Drive Systems, 2015, doi: 10.1109/peds.2015.7203522.

[11] B. Stumberger, G. Stumberger, D. Dolinar, A. Hamler, and M. Trlep, "Evaluation of saturation and cross-magnetization effects in interior permanent-magnet synchronous motor," IEEE Transactions on Industry Applications, vol. 39, no. 5, pp. 1264–1271, Sep. 2003, doi: 10.1109/tia.2003.816538.

[12] J. Neumann, C. Henaux, M. Fadel, D. Prieto, E. Fournier, and M. T. Yamdeu, "Geometrical parameters influence analysis on performance and incremental inductances of a Permanent Magnet Assisted Synchronous Reluctance Motor," in IECON 2019 - 45th Annual Conference of the IEEE Industrial Electronics Society, 2019.

[13] FEMM 4.2 user manual. Available: http://www.femm.info/wiki/Documentation/

[14] J. Neumann, C. Henaux, M. Fadel, D. Prieto, E. Fournier, and M. T. Yamdeu, "Analytical harmonic current model for a Permanent Magnet Assisted Synchronous Motor (PMa-SynRM) fed by PWM inverter," in EPE 2020 – 22nd European Conference on Power Electronics and Applications (EPE '20 ECCE Europe)

[15] T. A. Lipo, "Performance Calculations of a Reluctance Motor Drive by dq Harmonic Balance," IEEE Transactions on Industry Applications, vol. IA-15, no. 1, pp. 25–35, Jan. 1979.

[16] X. Chen, J. Wang, B. Sen, P. Lazari, and T. Sun, "A High-Fidelity and Computationally Efficient Model for Interior Permanent-Magnet Machines Considering the Magnetic Saturation, Spatial Harmonics, and Iron Loss Effect," IEEE Transactions on Industrial Electronics, vol. 62, no. 7, pp. 4044–4055, Jul. 2015.

VIII. BIOGRAPHIES

Jessica Neumann was born in São Bento do Sul, Brazil. She achieved a double degree in electrical engineering from ENSEEIHT INP in France and UFSC in Brazil in 2016 and 2017, respectively. Since 2018 she works on her PhD at the Laplace research laboratory in Toulouse, France. Her scholarship is funded under an industrial agreement with Leroy Somer - Nidec, Angoulême, France. Her research interests include electrical machines, power converters and control systems.

Carole Henaux received the Dipl. Ing. Degree in Electrical Engineering from ENSEEIHT, Toulouse, France, in 1992 and the PHD degree from the Institut National Polytechnique de Toulouse in 1996. She is now a Lecturer with the Electrical Engineering department of INPT / ENSEEIHT. She teaches Electrical Machines modeling and she works ate the GREM3 research group of INPT-ENSEEIHT-LAPLACE, Toulouse. The group in the fields of electromechanical energy conversion, with particular interest in novel techniques and design, methodologies such as electroactive materials, composite magnetic materials, electroactive fluids, analytical field calculation and optimal design.

Maurice Fadel (M'09) was born in Toulouse, France. He got the PhD degree at the Institut National Polytechnique de Toulouse in 1988, in the domain of the Control in Electric Engineering. He is currently a Professor in the Ecole Nationale Supérieure d'Electrotechnique, d'Electronique, d'Informatique, d'Hydraulique et des Télécommunications of Toulouse (ENSEEIHT). He works at Laboratoire Plasma et Conversion d'Energie (Laboratory of Plasma and Energy Conversion, LAPLACE). His field of scientific interest concerns the modeling and the control of the electric systems more especially of the synchronous machine, the control law of the static converters with the help of direct predictive controls approach and the definition of control strategies for cooperative systems.

Dany Prieto received the M.S. degree in Electrical Engineering from the University of Nantes, France, in 2011 and the Ph.D. degree from Centrale Supelec in 2015. Since 2015, he has been working with Leroy-Somer Motors as R&D Electrical Engineer. His research interests include permanent magnet synchronous machines and induction motors with their power electronic supply.

Etienne Fournier got his MSc in electrical engineering from Supélec Gif-sur-Yvette, France in 2012 and his PhD from the Laboratory of Plasma and Energy Conversion (LAPLACE) in 2015 in Toulouse, France. He currently works at Leroy Somer in Angoulême, France. His work focuses on preventive diagnostic of electrical machines under variable-speed control and power electronic converters.

Mathias Tientcheu Yamdeu received the M.Sc. degree in electrical engineering and automatic control from the National Polytechnic Institute of Toulouse (INP Toulouse), Toulouse, France, in 1990. He is currently a Senior Engineer with Leroy Somer in Angoulême, France, where he is in charge of the control and diagnostics of variable- speed drives and power electronic converters.